Cellulose (2018) 25:1309–1318
https://doi.org/10.1007/s10570-018-1658-x

ORIGINAL PAPER

Contribution of lignin to the surface structure and physical performance of cellulose nanofibrils film

Huiyang Bian · Ying Gao · Ruibin Wang · Zhulan Liu · Weibing Wu · Hongqi Dai

Received: 23 November 2017 / Accepted: 8 January 2018 / Published online: 12 January 2018
© Springer Science+Business Media B.V., part of Springer Nature 2018

Abstract Herein, lignocellulosic nanofibrils (LCNF) suspension containing 0.1, 3.9, and 17.2 wt% lignin were utilized to fabricate films by filtration and pressing process. The stiff nature of fibrils containing lignin made them less able to conform during filtration, resulting in more uneven surface structure with higher roughness value. Lignin in the films interfered in hydrogen bonding between cellulose nanofibrils, thus impairing mechanical property of the film, such as tensile stress and Young's modulus. Due to the presence of chromophore groups, lignin absorbed light and the light transmittance of film was decreased. However, the film containing lignin displayed unusually high hydrophobicity with water contact angle of 88° and maximal weight loss temperature (T_{max}) of 372 °C. Overall, this study provides useful knowledge for understanding the result of lignin on the formation, surface morphology and physical behavior of LCNF films, especially in related bioproducts that requires low hydrophilicity, high roughness and high thermal stability.

H. Bian · Y. Gao · Z. Liu · W. Wu · H. Dai (✉)
Jiangsu Co-Innovation Center of Efficient Processing and Utilization of Forest Resources, Nanjing Forestry University, Nanjing 210037, China
e-mail: hgdhq@njfu.edu.cn

R. Wang
School of Materials and Energy, Guangdong University of Technology, Guangzhou 510006, China

Keywords Lignin · Lignocellulosic nanofibrils · Film · Morphology · Mechanical property · Thermal stability · Hydrophobicity

Introduction

Cellulose nanofibrils (CNF), derived from various cellulose sources, is an interesting building block in composites, coatings, films, membranes, and packaging materials (Abdul Khalil et al. 2014; Alila et al. 2013; Nechyporchuk et al. 2016; Zhu et al. 2016). Films made from CNFs are of particular interest due to their mechanical robustness, large surface area and biodegradability (Kumar et al. 2014; Zhu et al. 2016). Most studies used lignin-free cellulose nanomaterials as the feedstock to produce CNF films (Qing et al. 2015; Wang et al. 2013). Because producing lignin containing cellulose nanomaterials such as LCNF is more environmental friendly by eliminating the usage of bleaching chemicals and results in higher yield than using bleached pulp fibers (Bian et al. 2017a). Furthermore, LCNF can be directly produced from raw lignocellulosic biomass using low cost and environmentally friendly fractionation without using commercial pulps (Bian et al. 2017b). Moreover, Lignin, composed of different kinds of phenylpropane units, is considered to be the glue that holds together other major biopolymers in plant biomass (Delgado-

Aguilar et al. 2016; Nair et al. 2017). It also can be used to adjust the polarity and hydrophilicity of cellulose. Therefore, it is reasonable to assume that the lignin maybe beneficial and an asset for LCNF film production.

A drawback of earlier research on preparing films was the fact that the precursor LCNF were obtained using high energy-consuming mechanical dissociation, and the LCNF diameter distributed unevenly, which limits large-scale utilization of LCNF. And although many studies discussed the physical, barrier, thermal and mechanical properties of LCNF films (Nair and Yan 2015; Rojo et al. 2015; Velásquez-Cock et al. 2016). There are no publicly available studies focusing on the surface structure and behavior of LCNF films. Spence et al. (2010a, b) studied the energy and chemical requirements in the production of lignin-containing nanopapers, which showed promising properties for packaging applications. The precise effect of lignin on the performance of LCNF was not clear, since different preparing methods were used in the respective investigations, making systematic analysis difficult. Rojo et al. (2015) addressed this issue by using SO_2-ethanol-water (SEW) fibers as raw material for LCNF film production. Nair and Yan (2015) investigated the effect of high lignin on the thermal properties of CNF and the performance of films as well as the influence of fibrillation process on LCNF thermal stability. However, these studies were limited since how lignin impact on the surface structure and property of films was not clearly comprehensively elucidated.

In this work, we used a recyclable maleic acid to depolymerize cellulose for producing LCNF containing different content of lignin to prepare LCNF films. The performance of these films, such as surface morphology, mechanical, and hydrophobicity properties, were evaluated and compared. The importance of this study is that these properties can be tailored to a specific application by controlling the Preparation conditions. For example, films without lignin may be most desirable for polymer reinforcement, while films with high lignin content may be more suitable for packaging and barrier materials.

Experimental

Materials

Three kinds of lignocellulosic nanofibrils were isolated using maleic acid hydrolysis followed by microfluidization as previously described in our work (Bian et al. 2017a). The pulp fibers were first reacted with maleic acid of 60 wt% concentration at 120 °C at 120 min. The hydrolyzed residual cellulosic solids were mechanically disintegrated using a microfluidizer (M-110EH, Microfludics Corp., Westwood, MA). For simplicity, the resulting nanofibers were referred thereafter as CNF, LCNF-LL and LCNF-HL, respectively.

Preparation of CNF and LCNF Films

CNF or LCNF suspensions were diluted to approximately 0.1 wt% and stirred at room temperature for 12 h to ensure well dispersed nanofibrils. Neat films were ultrafiltrated under air pressure of 50 psi in a hazardous waste filtration system (Millipore Corporation, USA) with a stainless steel cylinder. The filtration membrane was polyvinylidene difluoride (PVDF) membranes of 0.22-μm pore size (Millipore GVWP14250, Bedford, MA, USA) with a 142 mm diameter. After filtration, wet films were peeled from membrane and stacked between two filter papers (15 cm, slow, Fisher Scientific Inc., Pittsburgh, PA). The assembly was then sandwiched between two steel plates, and pressed by 23 kg weight at ambient temperature for 72 h.

Morphological characterization

The morphologies of films were observed using scanning electron microscopy (SEM, Carl Zeiss NTS, Peabody, MA) and atomic force microscopy (AFM workshop, Signal Hill, CA). For SEM analyses, films were pasted on well-polished aluminum mounts and sputter-coated with gold. Images were recorded using a Leo EVO 40 SEM under ultrahigh vacuum conditions. For AFM measurements, films were fixed on the mica wafer. Images were taken in vibrating mode at 160–225 kHz with a radius of the tip curvature of 10–15 nm.

Crystal structure

The crystalline structures of the starting materials and corresponding nanofibrils were determined using an X-ray diffractometer (Bruker D8 130 Discover Bruker Corp., Billerica, MA) equipped with Cu-Kα radiation in the 2θ range from 10° to 38° in steps of 0.02° . The crystallinity index (CrI) was calculated using the Segal method (Segal et al. 1959).

Specific surface area

Congo Red (CR) adsorption method was used to determine the specific area of cellulosic substrates in aqueous suspensions. Samples were adjusted a 100 mM phosphate buffer (pH = 6) and dyed with various concentrations of CR (10–30 wt% of the weight of substrate) at a final solids content of approximately 0.7%. Then these samples were incubated at 60 °C for 24 h. A small amount of NaCl (0.004 wt %) was added to each sample at the beginning of the experiment to neutralize charged surface sites on the original fiber and LCNF. After 24 h, the samples were centrifuged at 10,000 rpm for 10 min. Measurements of UV–Vis adsorption (Model 8453, Agilent Technologies, Inc., USA) at 500 nm of supernatant samples were taken to determine the maximum amount of CR adsorbed onto substrates using Eq. (1) derived from Langmuir's adsorption theory:

$$\frac{[E]}{[A]} = \frac{1}{K_{ad}A_{max}} + \frac{[E]}{A_{max}} \quad (1)$$

where $[E]$ (mg/mL) is the solution concentration of Congo Red at adsorption equilibrium, $[A]$ is the adsorbed amount of Congo red on the cellulose surface in mg/g (that reached a maximum value equivalent to A_{max}, the maximum adsorbed amount), and K_{ad} is the equilibrium constant. The specific surface area was determined using the following Eq. (2):

$$\mathrm{SSA} = \frac{A_{max} \times N \times SA}{MW \times 10^{21}} \quad (2)$$

where N is Avogadro's constant, SA is the surface area of a single dye molecule (1.73 nm^2), and MW is molecular weight (696 g/mole) of Congo Red.

Density and mechanical properties of films

The apparent density of the films was calculated by dividing sample basis weight by the apparent thickness. The basis weight and thickness was determined according to TAPPI standard T410 and TAPPI Method T411 (TAPPI 2002, 2010). Tensile tests were conducted using the T5002 MTS testing machine with a 500 N load cell, according to ASTM D638-10. The films were cut to conform to ASTM D638-10 type V dog bone shape using a special die (Qualitest, FL, USA). Prior to mechanical testing, specimens were pre-conditioned at 50% relative humidity and 23 °C for 1 week in a room. The specimens were pre-loaded with 5 N of force to remove slack, and the tests were performed with a crosshead speed of 1 mm/min. Five measurements were carried out for each sample and the averages were reported.

UV–Vis spectroscopic analysis

The visible light transmittance of films were measured using a UV–Vis spectrophotometer (Model 8453, Agilent Technologies, Inc, CA). Percent transmittance at 600 nm (T_{600}) was recorded. Film specimens were cut into rectangles with size of 30 mm × 9 mm (length × width) and placed in a 10 mm quartz cuvette. The instrument is equipped with a kinetic operation mode for continuously recording complete spectra in a frequency of every 10 s. Due to different thickness of films, the transmittance was normalized to a similar thickness, i.e., 10 μm, between duplicates, according to Beer–Lambert Eq. (3):

$$\varepsilon = C \log T/d \quad (3)$$

where ε is the molar absorptivity, T is the transmittance value, C is sample concentration in moles/L, and d is the specimen thickness in cm.

Thermogravimetric analysis (TGA)

Thermogravimetric analysis (TGA) of starting materials and films were employed based on Pyris 1 thermogravimetric analyzer (PerkinElmer, Inc., Waltham, MA). Samples were heated from 50 to 600 °C with a heating rate of 10 °C/min under an inert atmosphere of nitrogen at a gas flow of 20 mL/min.

Hydrophobicity

The dynamic water contact angle (WCA) of films was determined by performing the sessile drop method using a contact angle analyzer (Attention Theta, Biolin Scienfic, Inc. Stockholm, Sweden). A drop of distilled water of roughly 8 µL was automatically dispensed on the surface of the film from a micro syringe. Images of the water drop were recorded right at the instant when the drop touched the film surface. Curve fitting and data analysis were performed using the One Attension software provided with the instrument. Each measurement was conducted for 90 s, and an average value was presented.

Results and discussion

Properties of CNF and LCNF

AFM images and corresponding height distribution of CNF and LCNF have been shown in our previous work, the number-average heights were 13.4, 9.6 and 7.1 nm for CNF, LCNF-LL, and LCNF-HL, respectively (Bian et al. 2017a). XRD measurements indicated that BEP, two UHP fibers, as well as their resultant CNF or LCNF have two characteristic peaks at about 16.4° and 22.6° reflection planes of typical cellulose I structure, respectively (Jia et al. 2017). The diffraction patterns of CNF and LCNF were not different from that of starting materials, revealing that maleic acid hydrolysis did not alter the crystal structure (Fig. 1a). On the basis of the crystallinity index (CrI) values calculated from the XRD patterns, CNF with the lowest lignin content had the highest CrI of 80.3% than LCNF-LL (CrI of 76.2%) and LCNF-HL (CrI of 69.0%).

Specific surface area (SSA) of substrate was calculated by Congo red (CR) adsorption using Langmuir-type isotherms. Previous study has reported that the SSA of unbleached nanofibrillated cellulose (UN-NFC with lignin content of 2.7%) from unbleached birch pulp was 124 m^2/g, higher than corresponding CNF (SSA of 98 m^2/g) from bleaching pulp (Ferrer et al. 2012). Similar reports were described that SSA increased with higher residual lignin content (Spence et al. 2010b). A significant in SSA was observed when comparing CNF (68 m^2/g) from bleached hardwood (BHW) to LCNF (202 m^2/g) from unbleached hardwood (UBHW) depending on the lignin content in (L)CNF. In this study, the CR adsorption experiments revealed slightly highest SSA value of 379 m^2/g for LCNF-HL, compared with 315 and 320 m^2/g for CNF and LCNF-LL, respectively (Fig. 1b). These results could be related to the hydrophilic nature of fibers containing a high lignin content that may improve the adsorption of CR molecules on cellulose surface.

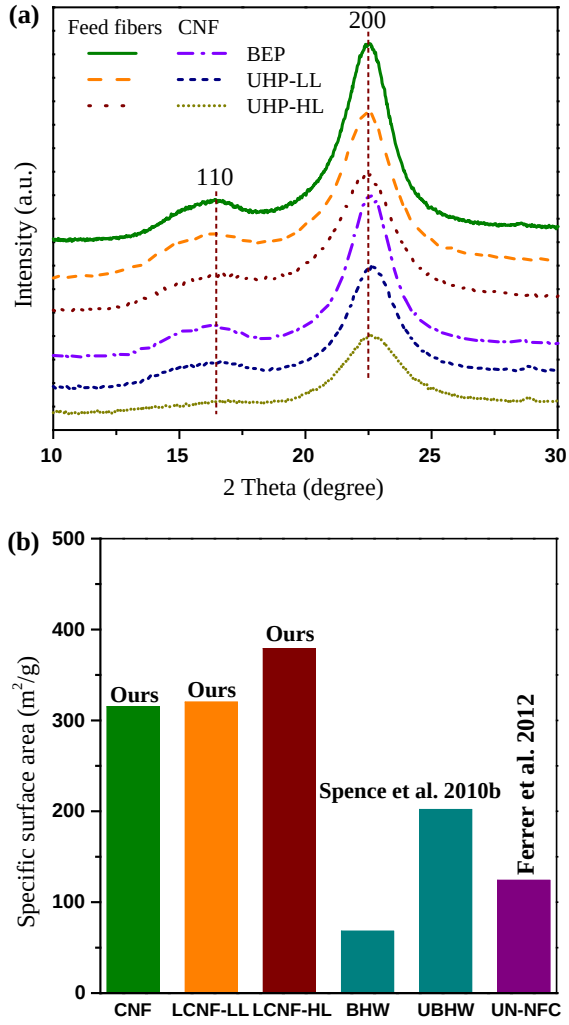

Fig. 1 **a** XRD patterns of starting materials and corresponding lignocellulosic nanofibrils, **b** comparison of specific surface area of different lignocellulosic nanofibril

Film morphology

It can been observed that a printed pattern placed underneath the CNF film seemed more clear than that of LCNF-HL film. In addition, they were flexible and did not show any sign of cracks or defects upon folding in Fig. 2. The surface and cross-sectional morphology of CNF, LCNF-LL, and LCNF-HL films were elucidated using SEM images. The well-dispersed cellulose nanofibrils in CNF film is apparent as almost no individual fibrils can be seen from the surface section (Fig. 2a), however, the presence of residual lignin within LCNF films made the surface uneven (Fig. 2b–c). Meanwhile, due to the hydrophobic property of lignin that resulted in comparatively poor dispersion of cellulose nanofibrils, the variation in the appearance of corresponding cross section was obviously different. A more compacted structure can be observed from the CNF film cross section, which was physically linked by more hydrogen bonding, compared to those LCNF films with many voids on the fractured interface (Fig. 2d–f).

To further investigate the influence of residual lignin on the plane view of films, AFM topographic and 3D images of the surface structure of different films were compared in Fig. 3, which allow us to propose a new model system describing the formation of lignocellulosic nanofiber films. It was found that the peak-to-valley height values were 335, 497 and 805 nm for CNF, LCNF-LL and LCNF-HL, respectively, from the AFM 3D images (Fig. 3d–f). Root mean surface (RMS) roughness value also can be a measure of film surface property, which is related to the diameter of fibrils and the degree of consolidation on the surface upon drying. As can been seen in Table 1, LCNF-HL film with high lignin content presented higher RMS roughness of 49.8 ± 4.7 nm, compared to LCNF-LL and CNF films with RMS roughness of 39.1 ± 2.6 and 29.9 ± 1.7 nm, respectively. These results differentiated from a previous work that fibrils with high lignin content formed smoother surface with lower RMS roughness (Rojo et al. 2015). It may be due to the different drying procedure of film. In our work, we fabricated film at room temperature for 2 days instead of the ultima hot-pressing at 100 °C for 2 h. Elevated temperature softened the amorphous lignin during pressing, and lignin was easy to fill the voids between the fibrils, resulting in smoother surface and lower RMS roughness. Room temperature was not able to achieve the above-mentioned results, therefore, rigid residual lignin led to uneven surface and high RMS roughness. The prepared LCNF films containing lignin may act as potential food packaging materials that require good barrier properties, such as low oxygen permeability and low water penetration.

Physical and mechanical property

The thickness, density and basis weight of different lignocellulosic nanofibril films were provided in Table 1. Samples that contained more lignin produced films with higher density and basis weight. All of the prepared films had a density of 1.422–1.529 g/cm^3, in agreement with the density value (0.96–1.52 g/cm^3) in the previous work (Kumar et al. 2014). Compared to the reported density of 1.6 g/cm^3, the lower density for all films indicated that the presence of empty space or pores among the fibrils in films. The presence of lignin between fibrils allowed more effective compaction during ultrafiltration, as a consequence, higher density and basis weight of 1.529 and 222 g/m^2, respectively, for LCNF-HL film were obtained.

Differences in mechanical properties of the various films were depicted in Fig. 4.

Mechanical properties mainly depend on single fibril and interfibril bonding, which can be affected by aspect ratio, chemical composition (cellulose, hemicellulose, lignin, protein, etc) or processing approach (Qing et al. 2013; Wang et al. 2013). Here we discuss the data in terms of the specific tensile stress and the specific Young's modulus as obtained by dividing the tensile stress and Young's modulus by density, respectively.

It can be seen the CNF film had the highest tensile stress and specific tensile stress of 115 MPa and 81 kN m/kg, respectively (Fig. 4a). However, both LCNF-LL and LCNF-HL films had lower tensile stress and specific tensile stress values of approximately 89 MPa and 59 kN m/kg. These results implied that lignin in films might interfere in hydrogen bonding between fibrils, thus weakening the interfibril bonds and resulting in low mechanical property. Young's modulus, which is calculated based on the initial linear region of the stress–strain curve, strongly depended on the crystallinity of nanofibrils (Qing et al. 2013). CNF films with the highest CrI of 80.3% had the highest value of 15 GPa of Young's modulus and 11 MN m/kg

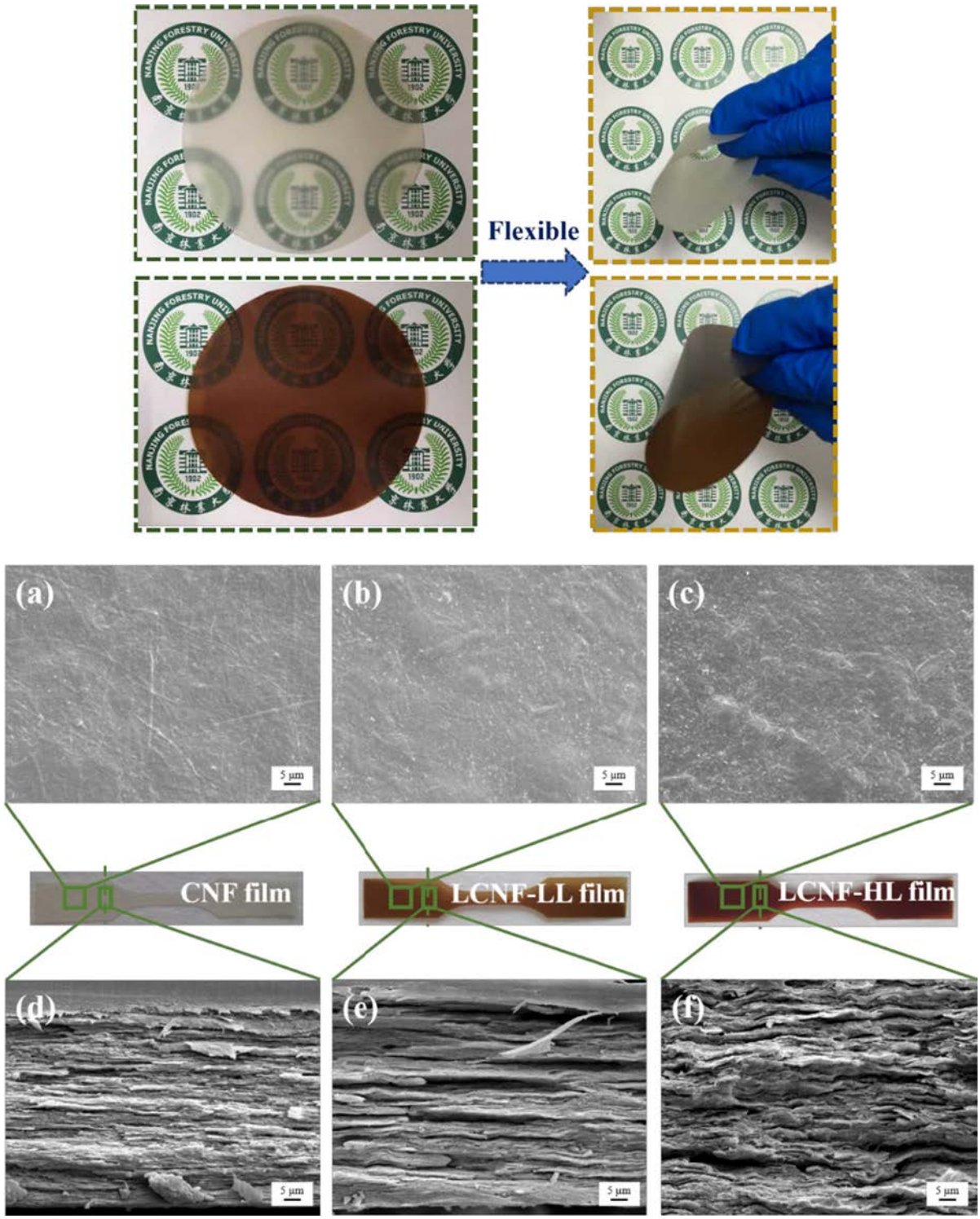

Fig. 2 Images of films made of CNF and LCNF-HL that show their optical transparency and flexibility. SEM images of the surface section (**a**–**c**) and the cross section (**d**–**f**) of films with different lignin content. *Scale bar* = 5 μm

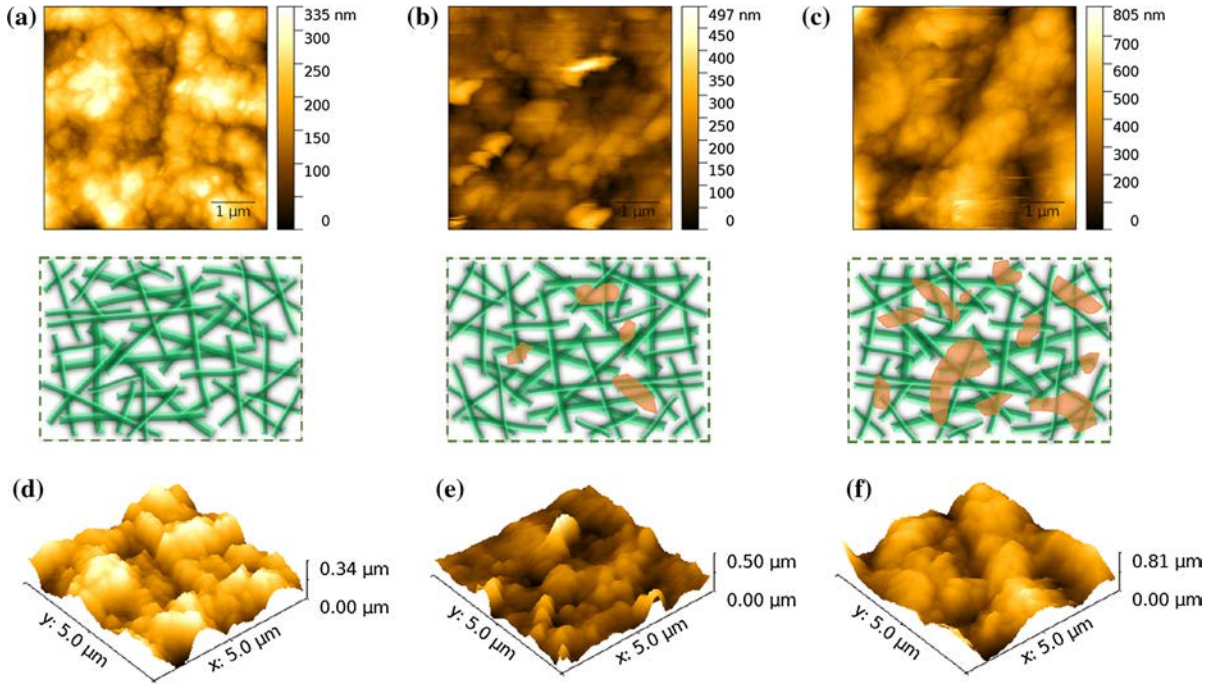

Fig. 3 AFM topographic (top panel) and 3D (bottom panel) images of different films, as well as proposed model (middle panel) to describe the distribution of lignin within films. *Scale bar* = 1 µm. **a–c** AFM topographic images of CNF film, LCNF-LL film and LCNF-HL film; **d–f** 3D images of CNF film, LCNF-LL film and LCNF-HL film

Table 1 Physical, optical, thermal and surface properties of CNF, LCNF-LL and LCNF-HL films

Film abbreviation	Thickness (µm)	Density (g/cm^3)	Basis weight (g/m^2)	RMS surface roughness (nm)	Normalized transmittance (%) at 600 nm	T_{onset} (°C)	T_{max} (°C)	Water contact angle (°)
CNF	121 ± 3	1.422	172	29.9 ± 1.7	45.2 ± 1.6	267	363	64.9 ± 1.0
LCNF-LL	123 ± 4	1.455	179	39.1 ± 2.6	37.3 ± 0.1	261	364	70.7 ± 0.4
LCNF-HL	146 ± 4	1.529	222	49.8 ± 4.7	31.0 ± 0.1	286	372	88.4 ± 0.5

RMS root mean square

of specific Young's modulus than other LCNF films (Fig. 4b). This is suggested that highly crystalline nanofibrils are the good candidates for reinforcing polymer composites.

Optical property

The use of transparent films and composites is of interest in many applications, so the light transmittance of CNF and LCNF films is compared. According to the Beer–Lambert Law, the absorption of light is exponentially reduced with the thickness, therefore, we normalized the films to a similar thickness, i.e., 10 µm before testing. The normalized light transmittance of CNF film at 600 nm was 45.2 ± 1.6, higher than 37.3 ± 0.1 and 31.0 ± 0.1 for LCNF-LL and LCNF-HL films, respectively. The decreased light transmittance can be ascribed to lignin, the main component contributing to the brownish wood color. Lignin in films can absorb light through chromophore groups, thereby reducing the light transmittance (Li et al. 2017).

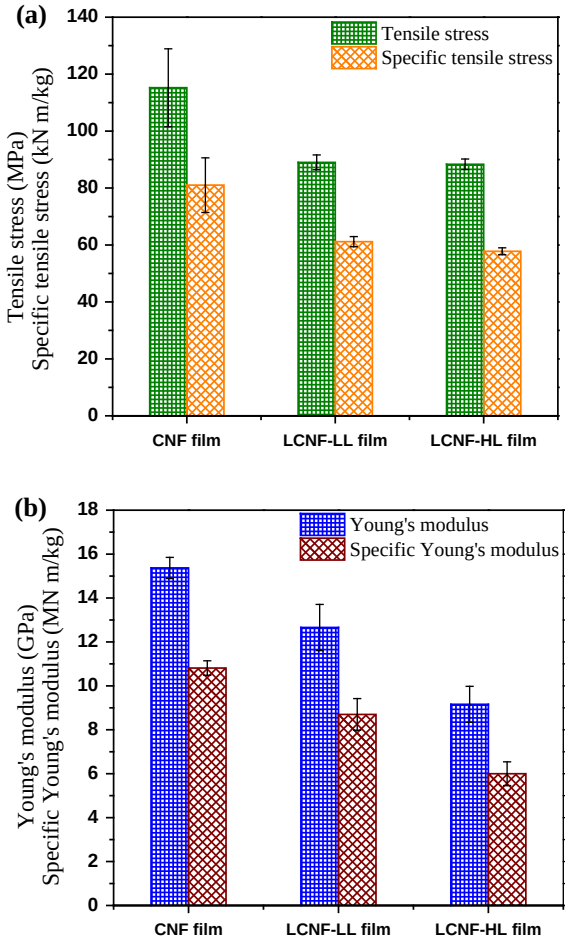

Fig. 4 Mechanical properties of different lignocellulosic nanofibril films. **a** Tensile stress and specific tensile stress; **b** Young's modulus and specific Young's modulus

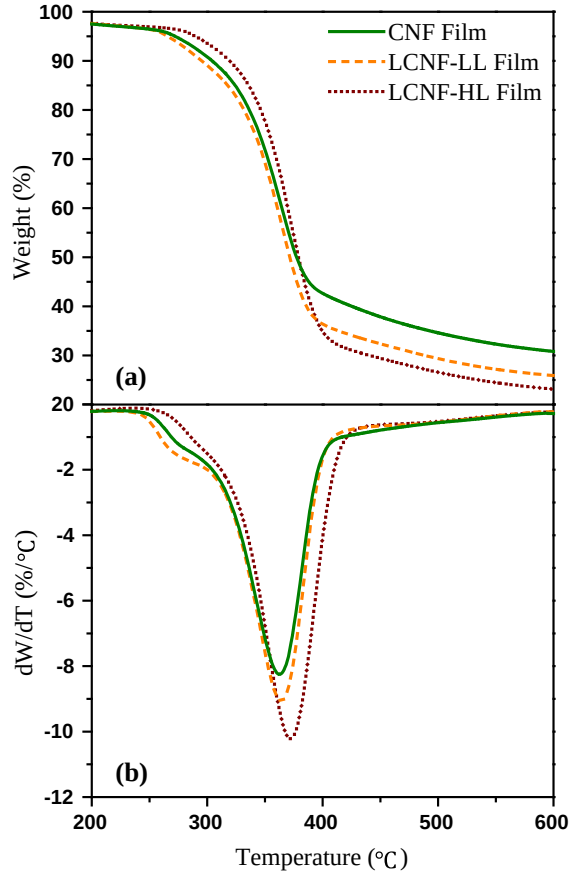

Fig. 5 Comparison of thermal stability of different lignocellulosic nanofibril films. **a** TGA weight loss; **b** TGA temperature derivative weight loss

Thermal property

The thermal stability and degradation behavior of cellulose nanomaterials is a very important parameter in biocomposite processing (Yu et al. 2013). The weight loss curves and the derivative of the weight loss curves versus temperature (dW/dT) of films were shown in Fig. 5a–b. The thermal transition of the films occurred in the range of 200–600 °C and included three phases: (1) moisture evaporation and decomposition of low-molecular-weight saccharides; (2) decomposition of cellulose; (3) decomposition of resides. Among the three samples, LCNF-HL films showed the highest onset degradation temperature (T_{onset}) of 286 °C and maximal weight loss temperature (T_{max}) of 372 °C derived from the derivated TGA data compared to the other two films (Table 1). The increased decomposition temperature for LCNF-HL film may be attributed to the presence of lignin, thermally more stable than other two primary components, cellulose and hemicelluloses. This indicates the advantage of using high lignin containing cellulose nanomaterials for bio-composite applications.

Hydrophobicity

The dynamic water contact angle (WCA) of films were measured by dropping water droplets on their surfaces, and averaged values were listed in Table 1. There are several factors closely related to the contact angle, including chemical composition, surface texture, surface chemistry, etc. of the tested materials (Chau et al. 2009). Herein, the existence of lignin might be the primary reason for the hydrophobicity seen in LCNF

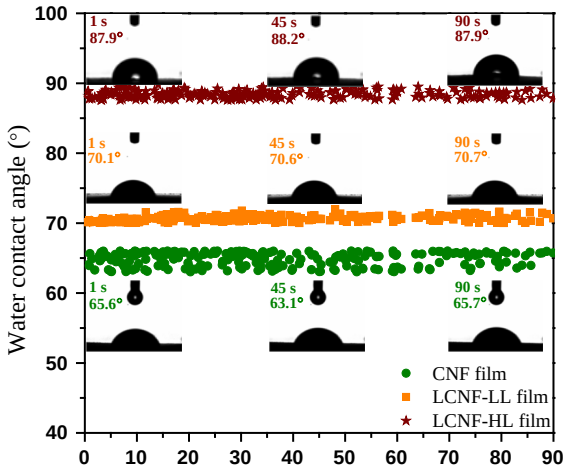

Fig. 6 Dynamic water contact angle of three lignocellulosic nanofibril films verse time, along with interaction images of the water angle droplet with film at 1, 45, and 90 s

film. Lignin in its native state is more hydrophobic compared to the hydrophilic cellulose and hemicellulose. High amount of lignin in films can shield the free accessible hydroxyl group from the formation of hydrogen bonding with water molecules (Nair and Yan 2015). As seen in Fig. 6, the average WCA was increased from 64.9 ± 1.0° for lignin free CNF film to 88.4 ± 0.5° for LCNF-HL film, suggesting that LCNF film exhibited excellent hydrophobicity. And the WCA of films remained constant as time increased, which manifested the stability of surface structure.

Conclusions

This work provided a route to tailor the surface morphology and physical performance of cellulosic nanofibrils films by controlling lignin content in films. The content and redistribution of the lignin on the surface of films significantly impacted the mechanical and physical properties of the resultant materials. The resulting lignin-free film possessed higher tensile stress and Young's modulus, while the resultant film with high lignin content not only leads to lower production cost by reducing bleaching chemicals but also exhibits excellent hydrophobicity. Overall, we have demonstrated the existence of lignin in films play an important role on nanopaper development, which can be relevant to areas where films require strength, hydrophobicity or thermal stability.

Acknowledgments This work was supported from the National Natural Science Foundation of China (Project No. 31470599) and the Doctorate Fellowship Foundation of Nanjing Forestry University. We would like to acknowledge Prof. Zhu of the Forest Product Lab for complimentarily providing us the LCNF samples.

References

Abdul Khalil HP, Davoudpour Y, Islam MN, Mustapha A, Sudesh K, Dungani R, Jawaid M (2014) Production and modification of nanofibrillated cellulose using various mechanical processes: a review. Carbohyd Polym 99:649–665. https://doi.org/10.1016/j.carbpol.2013.08.069

Alila S, Besbes I, Vilar MR, Mutjé P, Boufi S (2013) Non-woody plants as raw materials for production of microfibrillated cellulose (MFC): a comparative study. Ind Crops Prod 41:250–259. https://doi.org/10.1016/j.indcrop.2012.04.028

Bian H, Chen L, Dai H, Zhu JY (2017a) Integrated production of lignin containing cellulose nanocrystals (LCNC) and nanofibrils (LCNF) using an easily recyclable di-carboxylic acid. Carbohyd Polym 167:167–176. https://doi.org/10.1016/j.carbpol.2017.03.050

Bian H, Chen L, Gleisner R, Dai H, Zhu JY (2017b) Producing wood-based nanomaterials by rapid fractionation of wood at 80 °C using a recyclable acid hydrotrope. Green Chem 19:3370–3379. https://doi.org/10.1039/c7gc00669a

Chau TT, Bruckard WJ, Koh PT, Nguyen AV (2009) A review of factors that affect contact angle and implications for flotation practice. Adv Coll Interface Sci 150:106–115. https://doi.org/10.1016/j.cis.2009.07.003

Delgado-Aguilar M, González I, Tarrés Q, Pèlach MÀ, Alcalà M, Mutjé P (2016) The key role of lignin in the production of low-cost lignocellulosic nanofibres for papermaking applications. Ind Crops Prod 86:295–300. https://doi.org/10.1016/j.indcrop.2016.04.010

Ferrer A, Quintana E, Filpponen I, Solala I, Vidal T, Rodríguez A, Laine J, Rojas OJ (2012) Effect of residual lignin and heteropolysaccharides in nanofibrillar cellulose and nanopaper from wood fibers. Cellulose 19:2179–2193. https://doi.org/10.1007/s10570-012-9788-z

Jia C, Chen L, Shao Z, Agarwal UP, Hu L, Zhu JY (2017) Using a fully recyclable dicarboxylic acid for producing dispersible and thermally stable cellulose nanomaterials from different cellulosic sources. Cellulose 24:2483–2498. https://doi.org/10.1007/s10570-017-1277-y

Kumar V, Bollström R, Yang A, Chen Q, Chen G, Salminen P, Bousfield D, Toivakka M (2014) Comparison of nano- and microfibrillated cellulose films. Cellulose 21:3443–3456. https://doi.org/10.1007/s10570-014-0357-5

Li Y, Fu Q, Rojas R, Yan M, Lawoko M, Berglund L (2017) Lignin-retaining transparent wood. Chemsuschem 10:3445–3451. https://doi.org/10.1002/cssc.201701089

Nair SS, Yan N (2015) Effect of high residual lignin on the thermal stability of nanofibrils and its enhanced mechanical performance in aqueous environments. Cellulose 22:3137–3150. https://doi.org/10.1007/s10570-015-0737-5

Nair SS, Kuo P-Y, Chen H, Yan N (2017) Investigating the effect of lignin on the mechanical, thermal, and barrier properties of cellulose nanofibril reinforced epoxy composite. Ind Crops Prod 100:208–217. https://doi.org/10.1016/j.indcrop.2017.02.032

Nechyporchuk O, Belgacem MN, Bras J (2016) Production of cellulose nanofibrils: a review of recent advances. Ind Crops Prod 93:2–25. https://doi.org/10.1016/j.indcrop.2016.02.016

Qing Y, Sabo R, Zhu JY, Agarwal U, Cai Z, Wu Y (2013) A comparative study of cellulose nanofibrils disintegrated via multiple processing approaches. Carbohyd Polym 97:226–234. https://doi.org/10.1016/j.carbpol.2013.04.086

Qing Y, Sabo R, Wu Y, Zhu JY, Cai Z (2015) Self-assembled optically transparent cellulose nanofibril films: effect of nanofibril morphology and drying procedure. Cellulose 22:1091–1102. https://doi.org/10.1007/s10570-015-0563-9

Rojo E, Peresin MS, Sampson WW, Hoeger IC, Vartiainen J, Laine J, Rojas OJ (2015) Comprehensive elucidation of the effect of residual lignin on the physical, barrier, mechanical and surface properties of nanocellulose films. Green Chem 17:1853–1866. https://doi.org/10.1039/C4GC02398F

Segal L, Creely JJ, Martin AE, Conrad CM (1959) An empirical method for estimating the degree of crystallinity of native cellulose using the X-ray diffractometer. Text Res J 29:786–794

Spence KL, Venditti RA, Habibi Y, Rojas OJ, Pawlak JJ (2010a) The effect of chemical composition on microfibrillar cellulose films from wood pulps: mechanical processing and physical properties. Biores Technol 101:5961–5968. https://doi.org/10.1016/j.biortech.2010.02.104

Spence KL, Venditti RA, Rojas OJ, Habibi Y, Pawlak JJ (2010b) The effect of chemical composition on microfibrillar cellulose films from wood pulps: water interactions and physical properties for packaging applications. Cellulose 17:835–848. https://doi.org/10.1007/s10570-010-9424-8

TAPPI (2002) TAPPI standard test method (T410 om-02). Grammage of paper and paperboard

TAPPI (2010) TAPPI standard method (T411 om-10). Thickness (caliper) of paper, paperboard, and combined board

Velásquez-Cock J, Gañán P, Posada P, Castro C, Serpa A, Gómez HC, Putaux JL, Zuluaga R (2016) Influence of combined mechanical treatments on the morphology and structure of cellulose nanofibrils: thermal and mechanical properties of the resulting films. Ind Crops Prod 85:1–10. https://doi.org/10.1016/j.indcrop.2016.02.036

Wang Q, Zhu JY, Considine JM (2013) Strong and optically transparent films prepared using cellulosic solid residue recovered from cellulose nanocrystals production waste stream. ACS Appl Mater Interfaces 5:2527–2534. https://doi.org/10.1021/am302967m

Yu H, Qin Z, Liang B, Liu N, Zhou Z, Chen L (2013) Facile extraction of thermally stable cellulose nanocrystals with a high yield of 93% through hydrochloric acid hydrolysis under hydrothermal conditions. J Mater Chem A 1:3938–3944. https://doi.org/10.1039/c3ta01150j

Zhu HL, Luo W, Ciesielski PN, Fang ZJ, Zhu JY, Henriksson G, Himmel ME, Hu LB (2016) Wood-derived materials for green electronics, biological devices, and energy applications. Chem Rev 116(16):9305–9374. https://doi.org/10.1021/acs.chemrev.6b00225